ELSEVIER

Computers & Geosciences 32 (2006) 1182–1191

COMPUTERS & GEOSCIENCES

www.elsevier.com/locate/cageo

Parallel implementation of a velocity-stress staggered-grid finite-difference method for 2-D poroelastic wave propagation ☆

Dong-Hoon Sheen[a,b,*], Kagan Tuncay[a], Chang-Eob Baag[b], Peter J. Ortoleva[a]

[a]*Laboratory for Computational Geodynamics, Indiana University, Bloomington, IN 47405, USA*
[b]*School of Earth and Environmental Sciences, Seoul National University, San 56-1, Shillim-dong, Gwanak-gu, Seoul 151-747, Korea*

Received 6 January 2005; received in revised form 30 October 2005; accepted 2 November 2005

Abstract

Numerical simulation of wave propagation in poroelastic media demands significantly more computational capability compared to elastic media simulation. Use of serial codes in a single scientific workstation limits the size of problem. To overcome this difficulty, a parallel velocity-stress staggered-grid finite-difference method is developed for efficient simulation of wave propagation in 2-D poroelastic media. The finite difference formulation of Biot's theory has the properties of fourth order accuracy in space and second order accuracy in time. The model is decomposed into small subdomains for each processor. After each processor updates wavefields within its domain, the processors exchange the wavefields via message passing interface (MPI). The parallel implementation reduces the computational time and also allows one to study larger problems. From our numerical experiment, consistent with other 1-D experiments, it is found that the presence of heterogeneity of porous medium can produce significant P-wave attenuation in the seismic frequency range.

Keywords: Biot's theory; Poroelastic media; Wave propagation; Finite difference; Message passing interface (MPI)

1. Introduction

Seismic methods based on a single phase elastic or even a acoustic medium have been successfully applied to various geophysical problems to identify geological structures. In such studies, properties of a pore fluid such as density, bulk modulus, saturation and viscosity have been ignored. A porous medium, made of an elastic matrix filled with a viscous fluid, is a realistic model that allows one to account for the effects of pore fluid on the seismic properties of rocks. In recent years, numerical simulation of wave propagation in fluid saturated poroelastic media has received more attention as its importance in geophysical exploration and reservoir characterization is now recognized (Arntsen and Carcione, 2001; Pride et al., 2002; Sheen et al., 2003).

While attenuations from Biot's theory have been well known for decades, theoretical and numerical approaches to attenuations due to fine layering or

☆Code available at: http://seismic.snu.ac.kr/~sheen/porous/

*Corresponding author. School of Earth and Environmental Sciences, Seoul National University, San 56-1, Shillim-dong, Gwanak-gu, Seoul 151-747, Korea. Tel.: +82 28722713; fax: +82 28888696.

E-mail addresses: sheendh@snu.ac.kr (D.-H. Sheen), ktuncay@indiana.edu (K. Tuncay), baagce@snu.ac.kr (C.-E. Baag), ortoleva@indiana.edu (P.J. Ortoleva).

0098-3004/$ - see front matter © 2005 Elsevier Ltd. All rights reserved.
doi:10.1016/j.cageo.2005.11.001

heterogeneities of poroelastic structures have been developed in recent years (Gurevich et al., 1997; Shapiro and Muller, 1999; Pride et al., 2002). These studies showed that, even in the seismic frequency range, attenuation due to generation of the dissipative slow waves by randomly and finely layered poroelastic structure can significantly affect seismic wavefields.

Biot's theory (Biot, 1962) is the basis for the numerical simulation of wave propagation in fluid saturated poroelastic media. The finite-difference (FD) method for Biot's equations has been formulated in several ways, central difference FD method in displacement (Zhu and McMechan, 1991; Zeng et al., 2001), velocity-stress predictor-corrector FD method (Dai et al., 1995), and velocity-strain staggered-grid FD method (Zeng and Liu, 2001). Because central difference operators to perform first derivatives are less accurate than staggered-grid operators for high frequencies close to the Nyquist limit (Kneib and Kerner, 1993), we employ a staggered-grid operator to increase the accuracy of the numerical simulation. To simulate the wave propagation in unbounded media, the perfectly matched layer (PML) method (Berenger, 1994) is implemented as an absorbing boundary condition (ABC).

As PC clusters become an inexpensive alternative to "traditional" parallel computers, number of parallel numerical applications increases accordingly. The most efficient parallel implementations are ones which are optimized to balance the computational load and minimize the communication between processors. This can be easily achieved for an explicit FD method via domain decomposition. Each processor solve the problem within its small subdomain and at each time step communicates with neighboring processors to update wavefield information. The communication between processors is implemented by Message Passing Interface (MPI).

In this article, we present a numerical method to solve Biot's equations in 2-D heterogeneous, fluid saturated poroelastic media based on a first order hyperbolic formulation whose unknowns consist of solid phase velocity, velocity of fluid phase relative to that of solid phase, solid stress, and fluid pressure. Next, we present a methodology to parallelize this problem and show the performance of the parallelism. Finally, we consider a realistic situation for the heterogeneities, where the partial saturation is characterized by the von Karman autocorrelation function, and investigate attenuation due to the slow P wave in seismic frequencies.

2. Theory

Biot's theory (Biot, 1962) takes account of energy dissipation due to the relative motion between viscous pore fluid and the solid matrix. The theory predicts an additional compressional wave which was first confirmed by Plona (1980). The physical interpretations of the elastic constants in Biot's theory were provided by Biot and Willis (1957), Geertsma and Smit (1961) and Pride et al. (1992).

Biot's equations for a fluid-saturated, statistically isotropic, locally homogeneous, poroelastic medium are given by

$$\begin{aligned}\rho\ddot{\mathbf{u}} + \rho_f\ddot{\mathbf{w}} - (\lambda_c+\mu)\nabla\nabla\cdot\mathbf{u} - \mu\nabla^2\mathbf{u} - \alpha M\nabla\nabla\cdot\mathbf{w} = 0,\\ \rho_f\ddot{\mathbf{u}} + m\ddot{\mathbf{w}} + b\dot{\mathbf{w}} - \alpha M\nabla\nabla\cdot\mathbf{u} - M\nabla\nabla\cdot\mathbf{w} = 0,\end{aligned} \quad (1)$$

where $\mathbf{u}$ is the displacement vector for the solid, $\mathbf{w}$ the displacement vector for the fluid relative to that for the solid, ρ the overall density of the saturated medium determined by $\phi\rho_f + (1-\phi)\rho_s$, ρ_f and ρ_s the density of the fluid and the solid, ϕ the porosity, λ_c the Lamé constant of the saturated matrix, μ the shear modulus of the dry porous matrix, T the tortuosity, m the effective fluid density defined by $T\rho_f/\phi$, η the viscosity of the fluid, κ the permeability of the porous medium, b the mobility of the fluid defined by η/κ, K_s and K_f the bulk moduli of the solid and the fluid, K_b bulk modulus of the dry porous matrix, α the poroelastic coefficient of effective stress defined by $1-K_b/K_s$, M the coupling modulus between the solid and the fluid defined by $[\phi/K_f + (\alpha-\phi)/K_s]^{-1}$.

From the definition of strain energy function in porous media (Biot, 1962), the stress τ and the pore fluid pressure p are given by

$$\begin{aligned}\tau_{ij} &= 2\mu e_{ij} + \delta_{ij}(\lambda_c e_{kk} + \alpha M w_{k,k}),\\ p &= -\alpha M e_{kk} - M w_{k,k},\end{aligned} \quad (2)$$

where e_{ij} is the strain tensor defined by $(u_{i,j}+u_{j,i})/2$, δ_{ij} the Kronecker delta, $\delta_{ij}=0$ for $i\neq j$ and $\delta_{ij}=1$ for $i=j$, $w_{k,k}$ the spatial derivative, $\partial/\partial x_k$, and the summation convention is used:

$$e_{kk} = e_{ii} + e_{jj} \quad \text{and} \quad w_{k,k} = w_{i,i} + w_{j,j}.$$

The time derivatives of the displacement can be written in terms of the stress and the pore fluid

pressure:

$$(m\rho - \rho_f^2)\ddot{u}_i = m\tau_{ij,j} + \rho_f b\dot{w}_i + \rho_f p_{,i},$$
$$(m\rho - \rho_f^2)\ddot{w}_i = -\rho_f \tau_{ij,j} - \rho b\dot{w}_i - \rho p_{,i}. \quad (3)$$

These equations can be written as a set of first order differential equation in time domain by differentiating Eq. (2) with respect to time:

$$(m\rho - \rho_f^2)\dot{v}_i = m\tau_{ij,j} + \rho_f b V_i + \rho_f p_{,i},$$
$$(m\rho - \rho_f^2)\dot{V}_i = -\rho_f \tau_{ij,j} - \rho b V_i - \rho p_{,i},$$
$$\dot{\tau}_{ij} = \mu(v_{i,j} + v_{j,i}) + \delta_{ij}(\lambda_c v_{k,k} + \alpha M V_{k,k}),$$
$$\dot{p} = -\alpha M v_{k,k} - M V_{k,k}, \quad (4)$$

where $v_i = \dot{u}_i$ and $V_i = \dot{w}_i$. Eq. (4) forms a set of first order hyperbolic differential equations in time for v, V, τ, and p.

3. Finite-difference formulation

Eq. (4) can be discretized using a staggered-grid FD method (Levander, 1988; Graves, 1996). The most outstanding feature of this method is that the differential operators are all naturally centered at the same point in space and time (Fig. 1). The discretization yields

$$v_{x^{i+1/2,j}}^{n+1/2} = v_{x^{i+1/2,j}}^{n-1/2} + \mathrm{d}t[A_x(\Delta_x\tau_{xx} + \Delta_z\tau_{xz}) + B_x\overline{V}_x + C_x\Delta_x p]|_{i+1/2,j}^{n},$$

$$v_{z^{i,j+1/2}}^{n+1/2} = v_{z^{i,j+1/2}}^{n-1/2} + \mathrm{d}t[A_z(\Delta_x\tau_{xz} + \Delta_z\tau_{zz}) + B_z\overline{V}_z + C_z\Delta_z p]|_{i,j+1/2}^{n}, \quad (5)$$

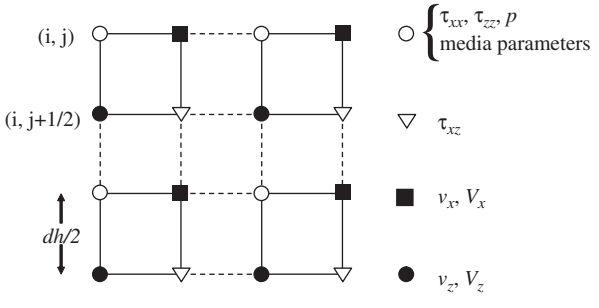

Fig. 1. Grid layout for staggered-grid formulation. Indices (i,j) represent spatial coordinates (x,z), respectively, and grid spacing dh is defined as a length between centers of two adjacent grid cells, modified from Graves (1996).

$$V_{x^{i+1/2,j}}^{n+1/2} = D_x V_{x^{i+1/2,j}}^{n-1/2} - \mathrm{d}t[E_x(\Delta_x\tau_{xx} + \Delta_z\tau_{xz}) + F_x\Delta_x p]|_{i+1/2,j}^{n},$$

$$V_{z^{i,j+1/2}}^{n+1/2} = D_z V_{z^{i,j+1/2}}^{n-1/2} - \mathrm{d}t[E_z(\Delta_x\tau_{xz} + \Delta_z\tau_{zz}) + F_z\Delta_z p]|_{i,j+1/2}^{n}, \quad (6)$$

$$\tau_{xx^{i,j}}^{n+1} = \tau_{xx^{i,j}}^{n} + \mathrm{d}t[(\lambda_c + 2\mu)\Delta_x v_x + \lambda_c\Delta_z v_z + \alpha M(\Delta_x V_x + \Delta_z V_z)]|_{i,j}^{n+1/2},$$

$$\tau_{zz^{i,j}}^{n+1} = \tau_{zz^{i,j}}^{n} + \mathrm{d}t[(\lambda_c + 2\mu)\Delta_z v_z + \lambda_c\Delta_x v_x + \alpha M(\Delta_x V_x + \Delta_z V_z)]|_{i,j}^{n+1/2},$$

$$\tau_{xz^{i+1/2,j+1/2}}^{n+1} = \tau_{xz^{i+1/2,j+1/2}}^{n} + \underline{\mu}_{xz}\,\mathrm{d}t[\Delta_z v_x + \Delta_x v_z]|_{i+1/2,j+1/2}^{n+1/2}, \quad (7)$$

and

$$p_{i,j}^{n+1} = p_{i,j}^{n} - \mathrm{d}t[\alpha M(\Delta_x v_x + \Delta_z v_z) + M(\Delta_x V_x + \Delta_z V_z)]|_{i,j}^{n+1/2}. \quad (8)$$

In the above equations, the superscripts denote the time step, and the subscripts denote the spatial indices. The symbol Δ represents the discrete form of the spatial differential operator, for example,

$$\Delta_x v_x|_{i,j} = \frac{27(v_{xi+1/2,j} - v_{xi-1/2,j}) - (v_{xi+3/2,j} - v_{xi-3/2,j})}{24dh}, \quad (9)$$

where dh denotes grid spacing. $\overline{V}$ denotes the arithmetic average in time domain, $(V^{n+1/2} + V^{n-1/2})/2$ and the coefficients A, B, C, D, E and F are defined as

$$A_x = \frac{\underline{m}_x}{(\underline{m}_x\underline{\rho}_x - \underline{\rho}_{f\,x}^2)},$$

$$B_x = \frac{\underline{\rho}_{f\,x}\underline{b}_x}{2(\underline{m}_x\underline{\rho}_x - \underline{\rho}_{f\,x}^2)}$$

$$C_x = \frac{\underline{\rho}_{f\,x}}{(\underline{m}_x\underline{\rho}_x - \underline{\rho}_{f\,x}^2)}$$

$$D_x = \frac{(2\underline{m}_x\underline{\rho}_x - 2\underline{\rho}_{f\,x}^2 - \underline{\rho}_{f\,x}\underline{b}_x\,\mathrm{d}t)}{(2\underline{m}_x\underline{\rho}_x - 2\underline{\rho}_{f\,x}^2 + \underline{\rho}_{f\,x}\underline{b}_x\,\mathrm{d}t)}$$

$$E_x = \frac{2\underline{\rho}_{f\,x}}{(2\underline{m}_x\underline{\rho}_x - 2\underline{\rho}_{f\,x}^2 + \underline{\rho}_{f\,x}\underline{b}_x\,\mathrm{d}t)}$$

$$F_x = \frac{2\underline{\rho}_x}{(2\underline{m}_x\underline{\rho}_x - 2\underline{\rho}_{f\,x}^2 + \underline{\rho}_{f\,x}\underline{b}_x\,\mathrm{d}t)}.$$

The effective media parameters yield a more accurate representation in the region near interfaces (Graves, 1996). The parameters are given by the harmonic average:

$$\underline{\rho}_x = \left[\frac{1}{2}\left(\frac{1}{\rho_{i,j}} + \frac{1}{\rho_{i+1,j}}\right)\right]^{-1},$$
$$\underline{\rho}_z = \left[\frac{1}{2}\left(\frac{1}{\rho_{i,j}} + \frac{1}{\rho_{i,j+1}}\right)\right]^{-1} \tag{10}$$

for the density. Similar averages are used for m, ρ_f, and b. The rigidity μ is given by

$$\underline{\mu}_{xz} = \left[\frac{1}{4}\left(\frac{1}{\mu_{i,j}} + \frac{1}{\mu_{i+1,j}} + \frac{1}{\mu_{i,j+1}} + \frac{1}{\mu_{i+1,j+1}}\right)\right]^{-1}. \tag{11}$$

Moczo et al. (2002) proposed a FD scheme based on a heterogeneous formulation of equations of motion for modeling seismic wave propagation in elastic media. They explicitly constructed heterogeneous displacement-stress FD scheme on a staggerd-grid with the volume harmonic averaging of the shear modulus and the bulk modulus, and volume arithmatic averaging of the density which is based on simplified boundary conditions inside heterogeneous media and which allows for an arbitrary position of the material discontinuity in the spatial grid. It is shown that this scheme is more accurate than other staggered-grid schemes. Therefore, incorporation of this for poroelastic media should be studied in a subsequent research.

4. Absorbing boundary condition

In order to simulate an unbounded medium, an ABC is often used to truncate the computational domain. A commonly used ABC in seismic modeling is the one-way wave equation based on the paraxial approximations of the acoustic or elastic wave equations (Clayton and Engquist, 1977). Recently, the PML method for electromagnetic problems has been proposed by Berenger (1994) and it has been successfully applied to various wave propagation problems (Chew and Weedon, 1994; Zeng and Liu, 2001).

Chew and Liu (1996) showed the effectiveness of the PML as an absorbing boundary condition for elastic waves. Using the concept of complex coordinates (Chew and Weedon, 1994) in the frequency domain with a time dependence of $\mathrm{e}^{-\mathrm{i}\omega t}$, the complex coordinate stretching variables can be written as

$$\tilde{x}_i = \int_0^{x_i} s_i(x_i')\,\mathrm{d}x_i', \quad s_i(x_i') = a_i^s + \mathrm{i}\omega_i^s/\omega, \tag{12}$$

where $a_i^s \geqslant 1$ is a scaling factor and $\omega_i^s \geqslant 0$ is an attenuation factor. The derivative $\partial/\partial\tilde{x}_i$ can be expressed in terms of the regular coordinate stretching variables, $\partial/\partial\tilde{x}_i = (1/s_i)\partial/\partial x_i$. In the PML region and the frequency domain, Eq. (4) becomes

$$\begin{aligned}
(-\mathrm{i}\omega)(m\rho - \rho_f^2)\hat{v}_i &= m\hat{\tau}_{ij,\tilde{j}} + \rho_f b\hat{V}_i + \rho_f\hat{p}_{,\tilde{i}},\\
(-\mathrm{i}\omega)(m\rho - \rho_f^2)\hat{V}_i &= -\rho_f\hat{\tau}_{ij,\tilde{j}} - \rho b\hat{V}_i - \rho\hat{p}_{,\tilde{i}},\\
(-\mathrm{i}\omega)\hat{\tau}_{ij} &= \mu(\hat{v}_{i,\tilde{j}} + \hat{v}_{j,\tilde{i}}) + \delta_{ij}(\lambda\hat{v}_{k,\tilde{k}} + \alpha M\hat{V}_{k,\tilde{k}}),\\
(-\mathrm{i}\omega)\hat{p} &= -\alpha M\hat{v}_{k,\tilde{k}} - M\hat{V}_{k,\tilde{k}},
\end{aligned} \tag{13}$$

where the hat refers to the frequency domain. The regular coordinate variable x_i is replaced by the complex coordinate stretching variable $\tilde{x}_i$,

$$(-\mathrm{i}\omega)(m\rho - \rho_f^2)\hat{v}_i = \frac{m}{s_j}\hat{\tau}_{ij,j} + \rho_f b\hat{V}_i + \frac{\rho_f}{s_i}\hat{p}_{,i}, \tag{14a}$$

$$(-\mathrm{i}\omega)(m\rho - \rho_f^2)\hat{V}_i = -\frac{\rho_f}{s_j}\hat{\tau}_{ij,j} - \rho b\hat{V}_i - \frac{\rho}{s_i}\hat{p}_{,i}, \tag{14b}$$

$$(-\mathrm{i}\omega)\hat{\tau}_{ij} = \mu\left(\frac{\hat{v}_{i,j}}{s_j} + \frac{\hat{v}_{j,i}}{s_i}\right) + \frac{\delta_{ij}}{s_k}(\lambda_c\hat{v}_{k,k} + \alpha M\hat{V}_{k,k}), \tag{14c}$$

$$(-\mathrm{i}\omega)\hat{p} = -\frac{\alpha M}{s_k}\hat{v}_{k,k} - \frac{M}{s_k}\hat{V}_{k,k}, \tag{14d}$$

To simplify the PML equations, the field variables are split as $v_j = v_j^{(k)}$ and $\tau_{ij} = \tau_{ij}^{(k)}$, where the superscript denotes the splitting direction. For example, Eq. (14a) for x component can be written as,

$$(-\mathrm{i}\omega)(m\rho-\rho_f^2)\hat{v}_x^{(x)}=\frac{m}{s_x}\hat{\tau}_{xx,x}+\rho_f b\hat{V}_x^{(x)}+\frac{\rho_f}{s_x}\hat{p}_{,x},$$
$$(-\mathrm{i}\omega)(m\rho-\rho_f^2)\hat{v}_x^{(z)}=\frac{m}{s_z}\hat{\tau}_{xz,z}+\rho_f b\hat{V}_x^{(z)}. \quad (15)$$

By taking the inverse Fourier transform, the PML equations in time domain are obtained:

$$(m\rho-\rho_f^2)(a_x^s\partial_t+\omega_x^s)v_x^{(x)}$$
$$=m\tau_{xx,x}+\rho_f b\left(a_x^sV_x^{(x)}+\omega_x^s\int_{-\infty}^{t}V_x^{(x)}\,\mathrm{d}t'\right)+\rho_f p_{,x},$$
$$(m\rho-\rho_f^2)(a_z^s\partial_t+\omega_z^s)v_x^{(z)}$$
$$=m\tau_{xz,z}+\rho_f b\left(a_z^sV_x^{(z)}+\omega_z^s\int_{-\infty}^{t}V_x^{(z)}\,\mathrm{d}t'\right). \quad (16)$$

Eqs. (14b)–(14d) can be transformed similarly.

To incorporate the PML boundary condition, the computational domain is divided into a PML region and an interior region. The outgoing waves are absorbed by the PML via high attenuation of the outgoing waves. Even though a perfectly matched interface generates no reflections at the interface, it cannot completely exclude reflections in discretized media due to discretization errors. The discretization error which generates fictitious reflection from outgoing waves is proportional to the grid spacing and the contrast between the two media (Chew and Jin, 1996). It has been known that the first few PMLs generate the most significant reflections, which forces the increments in attenuation properties in the first few PMLs to be small. On the contrary, insufficient attenuation may also cause reflections from the computational boundary, i.e., the outer boundary of the PML region. Therefore, the attenuation must be increased significantly toward the end of the PML region to guarantee the absorption of the outgoing waves.

In this work, the scaling factor and the attenuation factor have the following forms:

$$a_i^s=1+a_{\max}(l_i/L_{\mathrm{PML}})^n,$$
$$\omega_i^s=2\pi f_0\omega_{\max}(l_i/L_{\mathrm{PML}})^{n+\alpha}, \quad (17)$$

where l_i is the distance from the interface between the PML region and the interior region, L_{PML} is the thickness of the PML region, $a_{\max}$ and $\omega_{\max}$ are empirical coefficients and f_0 is the dominant frequency of the source. $a_{\max}$ and $\omega_{\max}$ control the rate of attenuation of the outgoing waves. Different rates of change of a_i^s and ω_i^s can lead to significant improvement of the PML performance (Rickard et al., 2003).

5. Source implementation

In this study, the first time derivative of the Gaussian function is used as the source time function:

$$F(t)=(t-t_0)\mathrm{e}^{-[\pi f_0(t-t_0)]^2}, \quad (18)$$

where t_0 is the time delay and f_0 is the dominant frequency. Since we are concerned with a composite material, a bulk source is used (Zhu and McMechan, 1991). The explosive source is partitioned linearly between the two phases by multiplying the source function by factors

$$W_s=(1-\phi), \quad W_f=\phi, \quad (19)$$

where W_s and W_f are the weighting factor for the solid normal stresses and fluid pressure, respectively, and ϕ is the porosity.

6. Domain decomposition

The computational domain is decomposed into relatively small subdomains which are assigned to each processor. It is important to divide subdomains evenly and minimize the communication between processors. Fig. 2 shows a typical 1-D and 2-D decomposition when 4 processors are used. Although computations in subdomains are same, generally 2-D decomposition is more efficient than 1-D decomposition. Thus, in our implementation, according to a given available processor number, 2-D decomposition has priority. If the number is less than 4 or a prime number, 1-D decomposition is applied.

In our approach, velocity and stress fields are staggered in spatial and time domain. Therefore, the velocity field is updated after the stress field is updated and vice versa. After each processor updates its own wavefields, the processors exchange wavefields at the edges of subdomains (see Fig. 2). For communications, a ghost layer whose thickness is 2 grid spacings at the edges of subdomains are used. The length of this ghost layer is equal to half of the length of spatial finite difference operator. The exchange of the wavefields in the PML region is the same as in the non-PML region because split wavefield variables have no spatial derivatives (see Eq. (16)). In the next section, we will show the performance of the parallelism.

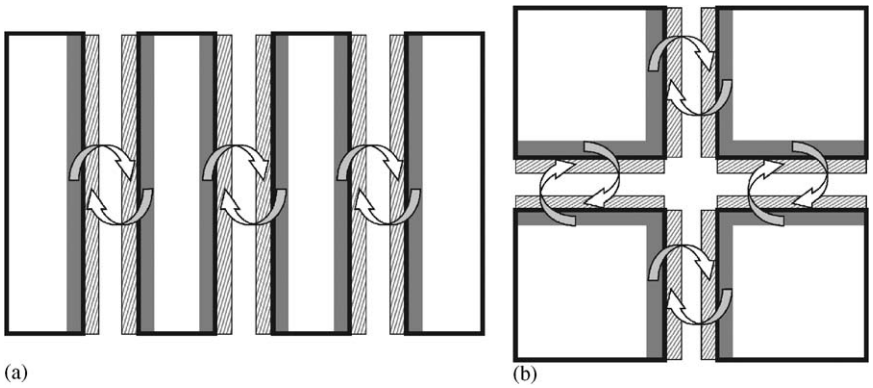

Fig. 2. Domain decomposition and communication between processors. (a) 1-D and (b) 2-D decomposition. Shaded and gray layers represent ghost layers and internal edges at subdomains, respectively.

Table 1
Physical properties of a gas-contact model

	Gas saturated layer	Water saturated layer
ρ (kg/m^3)	1.885×10^3	2.155×10^3
ρ_f (kg/m^3)	0.1×10^3	1.0×10^3
m (kg/m^3)	0.333×10^3	3.333×10^3
λ_c (GPa)	0.530	6.767
μ (GPa)	1.855	1.855
M (GPa)	7.323×10^{-2}	6.963
b (Pa s/m^2)	1.5×10^7	1.0×10^9
α	0.951	0.951
ϕ	0.3	0.3

7. Numerical examples

In the first example, we compare our numerical solution with the analytical solution given by Carcione and Quiroga-Goode (1996). The medium is homogeneous and acoustic. The pore fluid is considered as an ideal inviscid fluid. The other properties of the medium are those of gas saturated layer given in Table 1. An explosive bulk source with 45 Hz of dominant frequency is located at 50 m away from the receiver. Fig. 3 shows analytical and numerical responses of solid and fluid pressures. The agreement between analytical and numerical responses is very good. The first arrival is the P wave and the trailing wave is the slow P wave.

In the second example, we simulate a gas–water contact model (Dutta and Odé, 1983). This model has the same rock matrix in both gas and water saturated layers. The upper layer is gas saturated sandstone whereas the lower layer is water saturated sandstone, whose parameters are given in Table 1. Explosive bulk sources whose dominant frequencies are 45 Hz and 45 kHz are located at gas saturated layer. The size of the model is $N_x \times N_z = 600 \times 600$ nodes with 15 grids of PML on all sides of the computational boundary. The spatial grid spacings are 0.8 m and 0.8 mm whereas the time steps are 0.2 ms and 0.2 μs, respectively.

Fig. 4 shows vertical component snapshots of the solid velocity and the relative velocity of the fluid at $t = 0.2$ s and 0.2 ms, respectively. In this figure, P, P^s and S mean the P, slow P and S waves, respectively. The subscripts indicate the associated layer and multiple symbols represent reflected or transmitted waves. Incident P wave generates reflected and transmitted P and mode converted S waves (P_1P_1, P_1P_2, P_1S_1 and P_1Ss_2). Dutta and Odé (1983) showed that the P and S waves have weak dependence on frequency whereas the slow P wave shows strong dependence on frequency. At low frequencies, the slow P wave (P_1^s) is highly diffusive and disappears as a static mode at the source location (Fig. 4b). This is because the relative motion of the pore fluid at the low frequency range is of the Poiseuille type and the inertial term in Eq. (1), $m\ddot{\mathbf{w}}$, is negligible in comparison with the viscous term, $b\dot{\mathbf{w}}$ (Biot, 1956). However, at high frequencies, the slow P wave propagates (Figs. 4c and d). Incident slow P wave generates mode converted P and S waves ($P_1^sP_1$, $P_1^sS_1$, $P_1^sP_2$ and $P_1^sS_2$) and also reflected slow P wave ($P_1^sP_1^s$). One of the mode converted slow P waves ($P_1P_1^s$) is clearly shown whereas the other ($P_1P_2^s$) is not. The transmitted and mode converted slow P waves($P_1^sP_2^s$ and $P_1P_2^s$) in water saturated sandstone is not clear because the slow P wave is strongly attenuated in

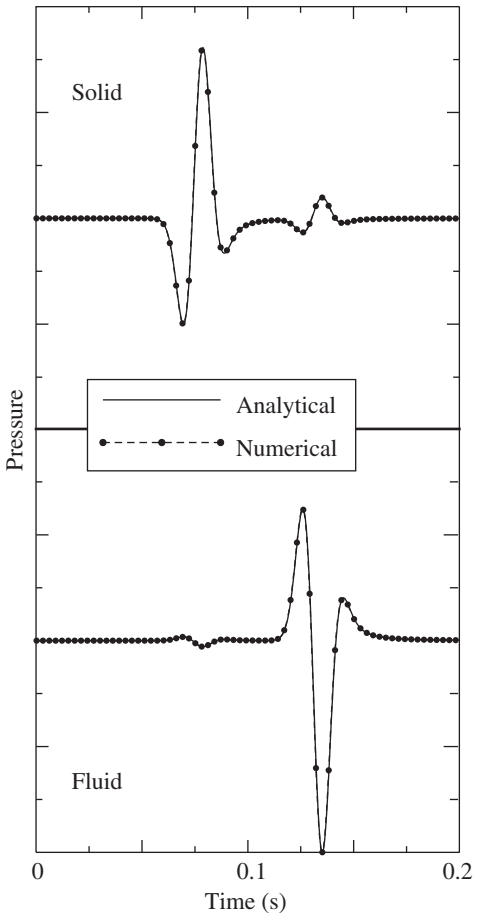

Fig. 3. Comparison of analytical and numerical waveforms of solid and fluid pressures. Upper and lower responses correspond to solid and fluid pressures, respectively. Pore fluid is an ideal inviscid fluid. Amplitudes are normalized with respect to a maximum of fluid pressure.

the lower layer where the fluid viscosity is higher. The lack of reflections from the computational boundary shows the effectiveness of the PML method.

The performance of a parallel algorithm is usually evaluated in terms of speedup or efficiency. Speedup is defined as the ratio of the elapsed time when executing a program on a single processor to the execution time when n processors are used:

$$S(n) = T_1/T_n. \tag{20}$$

Efficiency (E) measures the fraction of time and shows how all processors are utilized:

$$E(n) = S(n)/n = T_1/(T_n n). \tag{21}$$

If efficiency remains at 1 as more processors are added, it is called linear speedup. However, in general, the linear speedup is not achievable because of the communication between processors. To illustrate the performance of the approach, we used a simple model whose problem size is $N_x \times N_z = 600 \times 600$ grids and 1200 time steps were evaluated. We ran the simulations on an IBM SP cluster which contains 4 Power3$^+$ processors in a node. When only one processor is used, the simulation takes about 2078 s whereas it takes about 40 s with 64 processors. Fig. 5 shows the speedup, efficiency and elapsed time. Beyond 32 processors, although more processors are added, the efficiency decreases. Since the communication cost is greater than the computational cost, beyond a certain number of processors, the performance is hardly expected as much as processors are used. This suggests that the optimal number of processors depends on the problem size.

The scalability of an algorithm is also important in parallel computing because if an algorithm is scalable and the efficiency can be sustained as the number of processors is increased, the problem size can also be increased. Table 2 illustrates the scalability of the approach. Although the problem size is increased, the computation time is almost constant as the subdomain size is invariant.

When wavelengths are larger than layer thickness, it is shown that the slow P wave are generated in order to equilibrate the fluid pressure between the layers. The fluid flow associated with this equilibration can cause significant attenuation in the seismic frequency range (Pride et al., 2002). In the next example, attenuation due to the slow P wave in the seismic frequency range is investigated. We consider a heterogeneous model by introducing a transition layer between gas and water saturated sandstones whose saturation varies with depth (Fig. 6). The partial saturation is generated by von Karman autocorrelation function which defines random distributions of two different pore-filling fluids. For the construction of partially saturated layer, we follow a uniform distribution scheme from Helle et al. (2003). Another transition layer is introduced through the effective medium parameters to account for partial saturation (Bachrach and Nur, 1998). The material properties are same as above. The dominant frequency is 45 Hz. The spatial grid spacing is 0.1 m and the time step is 20 μs. In order to remove any small reflections from the computational boundary, we set the model size large enough so that the size is 640 × 640 m. The transition layer is 5 m thick. An explosive point source is placed at 80 m above the top of the transition layer. Two lines

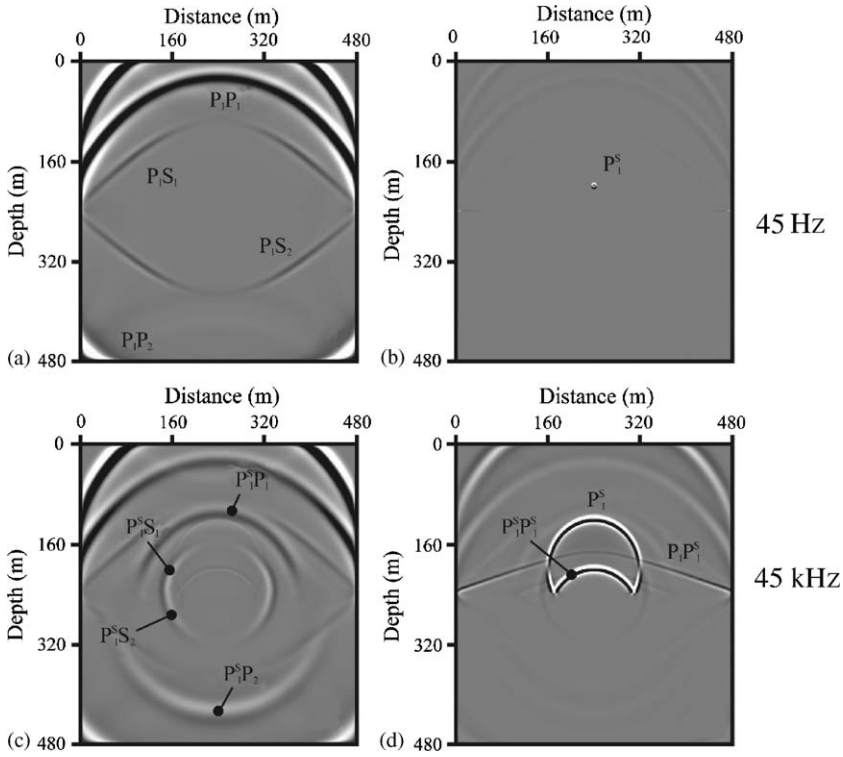

Fig. 4. Snapshots of vertical velocity component from a gas-water contact model (Dutta and Odé, 1983). (a) and (c) Snapshots of solid velocity; (b) and (d) Snapshots of relative fluid velocity (to solid velocity). P and S mean P and S waves, respectively. P^s denotes slow P wave. Subscripts indicate associated layers. Multiple symbols represent reflected or transmitted waves. Scaling for (b) is 20 times that for (a) and scalings for (c) and (d) are same.

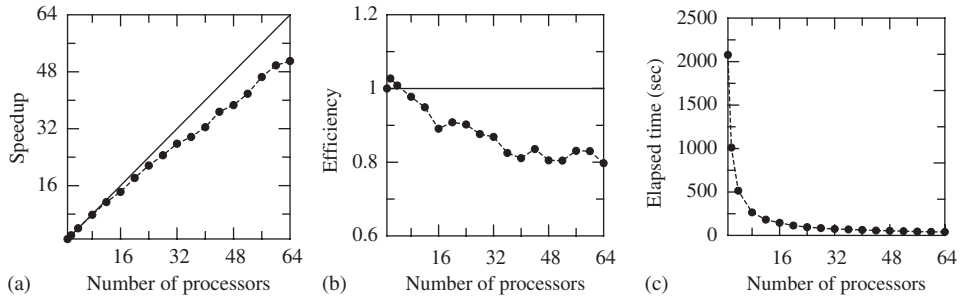

Fig. 5. Performance of algorithm. (a) Speedup, (b) Efficiency and (c) Elapsed time. Solid line is an "ideal" or linear speedup and dashed line is a performance of this approach. Circles indicate measured data points.

of receivers are located at 80 m above and below the top of the transition layer, whose offsets are from 1 to 100 m.

Fig. 7 shows the amplitude ratios of reflections and transmissions from the random medium to those from the effective medium. The direct arrivals in the reflection data are removed by differencing homogeneous responses. The P wave is separated by the divergence operator. The amplitude ratios are calculated with maximum amplitudes in frequency spectrums. Overall amplitude ratios are smaller than 1 in both reflection and transmission ratios. This suggests that attenuation due to the dissipative slow waves in heterogeneous poroelastic structure significantly affects seismic wavefields in the seismic frequency range.

Table 2
Elapsed time for fixed-size decomposition in a processor[a]

Problem size	# of processors	Elapsed time (s)
600 × 600	1	2078.17
1200 × 600	2	2060.77
1200 × 1200	4	2020.57
2400 × 1200	8	2039.63
2400 × 2400	16	2055.73
4800 × 2400	32	2053.47
3600 × 3600	36	2097.63
4800 × 3600	48	2124.94
4800 × 4800	64	2168.51

[a]Each processor has the same size of subdomain.

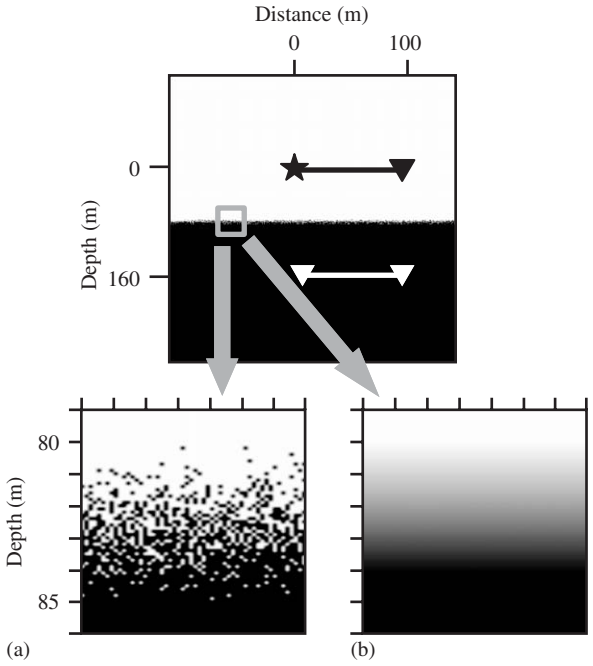

Fig. 6. Gas–water contact models with transition layers. (a) random transition layer and (b) uniform transition layer.

8. Conclusion

A parallel implementation of velocity-stress staggered-grid FD method to solve Biot's equations in fluid saturated poroelastic media is presented. Parallelism is accomplished by domain decomposition via message passing interface (MPI). It is shown that a significant speedup is obtained with a moderate number of processors. The scalability of this algorithm allows for the problem size to be increased as the number of processors is increased.

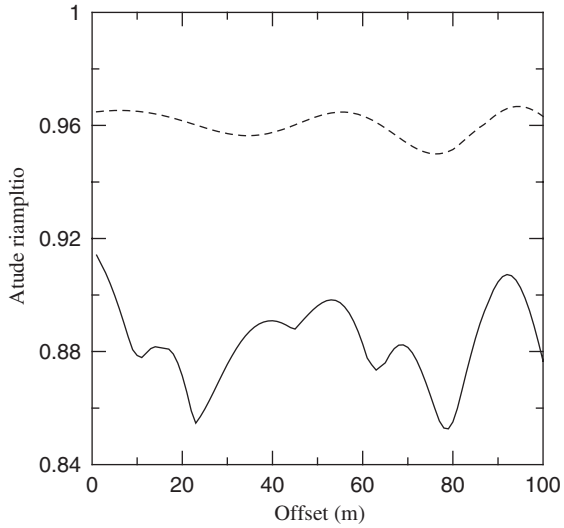

Fig. 7. Amplitude ratios from transition layer models (Fig. 6). Dashed and solid lines represent transmissions and reflections, respectively.

In numerical examples, we have shown that poroelastic wave phenomena in heterogeneous media can be simulated efficiently with this method. We have verified that attenuation in heterogeneous poroelastic media can be significant even in the seismic frequency range due to the slow P wave, which have been investigated in finely layered model (Gurevich et al., 1997; Pride et al., 2002). Therefore, it is believed that the comprehensive study of poroelastic wave propagation provides a methodology for the seismic analysis of reservoir characterization.

Acknowledgements

This work was partially supported by a grant from the Office of Science (# DE-F602-91ER14175), a contract from the Office of Fossil Energy (# DE-RA26-99FT40160) of the United States Department of Energy and the BK21 program through the School of Earth and Environmental Sciences, Seoul National University.

References

Arntsen, B., Carcione, J.M., 2001. Numerical simulation of the biot slow wave in water-saturated nivelsteiner sandstone. Geophysics 66, 890–896.

Bachrach, R., Nur, A., 1998. High-resolution shallow-seismic experiments in sand part i: Water table fluid flow and saturation. Geophysics 63, 1225–1233.

Berenger, J.P., 1994. A perfectly matched layer for the absorption of electromagnetic waves. Journal of Computational Physics 114, 185–200.

Biot, M.A., 1956. Theory of propagation of elastic waves in a fluid-saturated porous solid. i. low-frequency range. The Journal of the Acoustical Society of America 28, 168–178.

Biot, M.A., 1962. Mechanics deformation and acoustic propagation in porous media. Journal of Applied Physics 33, 1482–1498.

Biot, M.A., Willis, D.G., 1957. The elastic coefficients of the theory of consolidation. Journal of Applied Mechanics 24, 594–601.

Carcione, J.M., Quiroga-Goode, G., 1996. Full frequency-range transient solution for compressional waves in a fluid-saturated viscoacoustic porous medium. Geophysical Prospecting 44, 99–129.

Chew, W.C., Jin, J.M., 1996. Perfectly matched layers in the discretized space: an analysis and optimization. Electromagnetics 60, 325–340.

Chew, W.C., Liu, Q.H., 1996. Perfectly matched layers for elastodynamics: a new absorbing boundary condition. Journal of Computational Acoustics 4, 72–79.

Chew, W.C., Weedon, W.H., 1994. A 3-d perfectly matched medium from modified maxwell's equations with stretched coordinates. Microwave and Optical Technology Letters 7, 599–604.

Clayton, R., Engquist, B., 1977. Absorbing boundary conditions for acoustic and elastic wave equations. Bulletin of the Seismological Society of America 67, 1529–1540.

Dai, N., Vafidis, A., Kanasewich, E.R., 1995. Wave propagation in heterogeneous, porous media: a velocity-stress, finite-difference method. Geophysics 60, 327–340.

Dutta, N.C., Odé, H., 1983. Seismic reflections from a gas–water contact. Geophysics 48, 148–162.

Geertsma, J., Smit, D.C., 1961. Some aspects of elastic wave propagation in fluid-saturated porous solids. Geophysics 26, 169–181.

Graves, R.W., 1996. Simulating seismic wave propagation in 3d elastic media using staggered-grid finite difference. Bulletin of the Seismological Society of America 86, 1091–1106.

Gurevich, B., Zyrianov, V.B., Popatnikov, S.L., 1997. Seismic attenuation in finely layered porous rocks: effects of fluid flow and scattering. Geophysics 62, 319–324.

Helle, H.B., Pham, N.H., Carcione, J.M., 2003. Velocity and attenuation in partially saturated rocks: poroelastic numerical experiments. Geophysical Prospecting 51, 551–566.

Kneib, G., Kerner, C., 1993. Accurate and efficient seismic modeling in random media. Geophysics 58, 576–588.

Levander, A.R., 1988. Fourth-order finite-difference p-sv seismograms. Geophysics 53, 1425–1436.

Moczo, P., Kristek, J., Vavrycuk, V., Archuleta, R.J., Halada, L., 2002. Third heterogeneous staggered-grid finite-difference modeling of seismic motion with volume harmonic and arithmetic averaging of elastic moduli and densities. Bulletin of the Seismological Society of America 92, 3042–3066.

Plona, T.J., 1980. Observation of a second bulk compressional wave in a porous medium at ultrasonic frequencies. Applied Physics Letters 36, 259–261.

Pride, S.R., Gangi, A.F., Morgan, F.D., 1992. Deriving the equations of motion for porous isotropic media. The Journal of the Acoustical Society of America 92, 3278–3290.

Pride, S.R., Tromeur, E., Berryman, J.G., 2002. Biot slow-wave effects in stratified rock. Geophysics 67, 271–281.

Rickard, Y.S., Georgieva, N.K., Huang, W.-P., 2003. Application and optimization of pml abc for the 3-d wave equation in the time domain. IEEE Transactions on Antennas and Propagation 51, 286–295.

Shapiro, S.A., Muller, T.M., 1999. Seismic signatures of permeability in heterogeneous porous media. Geophysics 64, 99–103.

Sheen, D.-H., Tuncay, K., Baag, C.-E., Ortoleva, P.J., 2003. Wave propagation in poroelastic media: a velocity-stress staggered-grid finite-difference method with perfectly matched layers. In: 73rd Annual meeting. Society of Exploration Geophysicists, Dallas, TX, pp. 2295–2298.

Zeng, Y.Q., Liu, Q.H., 2001. A staggered-grid finite-difference method with perfectly matched layers for poroelastic wave equations. The Journal of the Acoustical Society of America 109, 2571–2580.

Zeng, Y.Q., He, J.Q., Liu, Q.H., 2001. The application of the perfectly matched layer in numerical modeling of wave propagation in poroelastic media. Geophysics 66, 1258–1266.

Zhu, X., McMechan, G.A., 1991. Numerical simulation of seismic responses of poroelastic reservoirs using biot theory. Geophysics 56, 328–339.